Hindawi
Journal of Nanomaterials
Volume 2018, Article ID 9425938, 9 pages
https://doi.org/10.1155/2018/9425938

Research Article

Structural, Optical, and Photocatalytic Activities of Ag-Doped and Mn-Doped ZnO Nanoparticles

Mengstu Etay Ashebir[1], **Gebrekidan Mebrahtu Tesfamariam**[1], **Gebretinsae Yeabyo Nigussie**[1] and **Tesfakiros Woldu Gebreab**[2]

[1]*Department of Chemistry, College of Natural and Computational Sciences, Mekelle University, Mekelle, Ethiopia*
[2]*Department of Physics, College of Natural and Computational Sciences, Mekelle University, Mekelle, Ethiopia*

Correspondence should be addressed to Mengstu Etay Ashebir; mengstuetay@gmail.com

Received 12 April 2018; Revised 26 June 2018; Accepted 24 July 2018; Published 3 September 2018

Academic Editor: Giuliana Magnacca

We report the photocatalytic activities of ZnO, Ag-doped ZnO, and Mn-doped ZnO nanoparticles (NPs). Ag-doped and Mn-doped ZnO samples were synthesized using a coprecipitation method and calcined at 600°C. XRD, SEM, EDX, and UV-vis spectroscopy techniques were employed for characterization of the synthesized samples. The photocatalytic activities of the samples were evaluated by measuring the photocatalytic decolorization of methyl violet with sunlight being the source of energy. XRD patterns of the samples confirmed the wurtzite structure without change which was indicative of the absence of Mn- and Ag-related secondary phases for the doped ZnO. The UV-vis spectra indicated the band gap energy of ZnO, Ag-doped ZnO, and Mn-doped ZnO to be 2.98, 2.80, and 2.64 eV, respectively. Photocatalytic decolorization of methyl violet for the synthesized samples was found to be favorable at a pH of 9.0, catalyst dose of 1 g/L, and initial dye concentration of 4.5×10^{-4} g/L. Mn-doped ZnO and Ag-doped ZnO photocatalytic decolorization efficiency was significantly higher than undoped ZnO. Incorporation of Mn and Ag enhanced the visible-light photocatalytic activity of ZnO; this could be due to the ability of these metals to increase the surface defects of ZnO which in turn shift their optical absorption towards the visible region.

1. Introduction

Currently, industrial effluents and household wastewater that are improperly disposed into the environment are becoming the major sources of residual dye pollutants [1]. Wastewater contaminated with residual dyes from textile industries, paper industries, and other industries are among the main sources of environmental pollutants in both developed and developing countries. Such industries produce a lot of organic contaminants including dyes such as methyl violet (MV) which is toxic as it can cause severe skin, respiratory, gastrointestinal tract, and eye irritations [2]. The toxic and potentially carcinogenic substances coming from these dyes cause severe environmental and health problems when they are released into the aquatic environment [3].

Numerous studies have been conducted to develop methods and technologies for the removal of residual dyes from wastewater which can be classified as physical, biological, and chemical methods. Physical methods include membrane filtration, adsorption, and precipitation [4], biological methods include biodegradation processes to remove bacteria used for the degradation of soluble organic matter present in effluent, and chemical methods include photochemical decolorization, chlorination, and ozonation [5]. These conventional ways for treatment of wastewater, such as adsorption, chemical precipitation, separation, and coagulation which merely transfer dyes from one phase to another are not effective methods, because they bring secondary pollution.

Nowadays, the use of metal oxide nanoparticles for water treatment has gained special attention. This is due to their cost-effectiveness, stability, recyclability, and environmental friendliness as photocatalysts [6]. Surface area and surface defects play a significant role in enhancing the photocatalytic activities of metal oxides. The reason is that doping of metal oxides with metal and/or transition metals increases the

surface defects, affects the optical and electronic properties, and shifts the optical absorption towards the visible region [7].

ZnO has been known to be one of the desired NPs for photocatalytic degradation of inorganic and organic contaminants in various matrices. This is due to its high photosensitivity, harmlessness, low cost, and chemical stability [8, 9]. Most semiconductor photocatalysts like ZnO has a band gap energy in the range of the ultraviolet region, which is ≥3.2 eV [10]. Thus, semiconductors enhance photocatalysis with UV radiation. Unfortunately, the sunlight spectrum includes only about 5–7% of UV light [11]. This minimum amount of UV light in the sunlight spectrum has particularly ruled out the use of the natural source of light for photocatalytic decolorization of pollutants.

Methyl violet (MV) is a cationic dye which has an aromatic structure which is resistant to light and biological activity [2]. It has a variety of uses in the textile and leather industries, as well as in processing paper and pulp. The release of the dye to the environment causes toxicity problems. Long-term exposure to the dye causes mutagenic, carcinogenic, and allergic effects [12]. Thus, in this study, the photocatalytic decolorization of the MV dye has been investigated. In this paper, the synthesis of ZnO, Ag-doped ZnO, and Mn-doped ZnO NPs through the precipitation method and their photocatalytic decolorization activities using MV as a model have been reported.

2. Experiments

2.1. Materials. All chemicals used were analytical grade and used without further purification. These chemicals include zinc chloride ($ZnCl_2$, Sigma-Aldrich), anhydrous manganese (II) chloride ($MnCl_2$, Sigma-Aldrich), silver nitrate ($AgNO_3$, Sigma-Aldrich), ammonia water (NH_4OH, Sigma-Aldrich), sodium hydroxide (NaOH, Sigma-Aldrich), ethanol (C_2H_5OH, 99.5%, Sigma-Aldrich), acetone, and distilled water.

2.2. Synthesis of ZnO, Ag-Doped ZnO, and Mn-Doped Nanoparticles. The ZnO nanoparticle was synthesized from $ZnCl_2$ through the precipitation method. 1 mol of $ZnCl_2$ was added to a beaker and dissolved in 100 mL of distilled water with continuous stirring. A 10% NaOH solution was added into the beaker dropwise until the pH became 12. During the addition of the NaOH solution, white precipitates were formed and finally, the sedimentation process was finished at pH 12. The precipitates were washed many times with deionized water and separated through a separatory funnel and centrifuged until free of impurities. The purified white precipitate was dried for 24 hours at 80°C. At this point, the white product did not show high crystallinity because it consisted of ZnO and $Zn(OH)_2$. Then, it was calcined at 600°C for 3 hours, to allow for the complete removal of inorganic matter and to obtain highly crystallized ZnO NPs. The resulting precipitate was washed with ethanol and centrifuged (4000 rpm). The above procedure was repeated five times to remove unreacted ions. The synthesized NPs were then used for further experimental exploration, adapted from [13] with some modifications.

To prepare Mn-doped ZnO NPs, 0.95 mol of $ZnCl_2$ and 0.05 mol of $MnCl_2$ were mixed in a beaker, and dissolved in 100 mL of distilled water with continuous stirring until the homogeneous solution was formed. 25–30% of aqueous ammonia was added slowly into the solution to get sedimentary products until the pH of solutions became 8.5. When the reaction of the precursors and ammonia was completed, the precipitate was collected via centrifugation from the solution. The precipitated products were washed with diethyl ether in the fume hood and then washed using 99.9% purity ethanol. As a final point, it was washed three times with deionized water and centrifuged. Finally, it was dried at 80°C for 24 h and calcined at 600°C for 2 h under normal atmospheric conditions, and nanoparticle products were obtained [13].

To prepare Ag-doped ZnO NPs, 0.95 mol of $ZnCl_2$ and 0.05 mol of $AgNO_3$ were mixed to 100 mL of distilled water; aqueous ammonia was added drop by drop until a pH of 7 was attained with continuous stirring for 30 min. The white gel produced was allowed to settle overnight. For the complete elimination of impurities, the precipitate formed was washed with deionized water and acetone followed by centrifugation at 3500 rpm. The precipitate was then kept in an oven at 80°C for 24 h to obtain a dry powder which was then subjected to calcination at 600°C for 2 h in a muffle furnace fitted with a PID temperature controller with the heating rate kept at $10^{\circ}C\,min^{-1}$ [14].

2.3. Characterization. X-ray diffraction (XRD) measurements of all the samples were carried out using the Shimadzu X-ray diffractometer with Cu-Kα radiation ($\lambda = 1.5406$ Å) and a scan speed of 3.00 deg/min. The scanning electron microscopy (SEM) study was carried out by a JEOL JSM-5610 equipped with a BE detector scanning electron microscope. The energy dispersive X-ray (EDX) spectrum was recorded with the JEOL JSM-5610 SEM equipped with EDX. UV-vis spectra of the oxides were recorded employing a PerkinElmer Lamda 35 spectrometer used to estimate the absorbance edge which is operated at a wavelength range of 200–800 nm in diffuse reflectance mode. Spectra were recorded at room temperature, and the data were transformed through the Kubelka-Munk function [15].

2.4. Photocatalytic Testing. In laboratory scale, numerous methods for the heterogeneous photocatalytic decolorization of dyes have been investigated. In this work, the MV dye was selected as the model chemical for the evaluation of the photocatalytic efficiency of the silver- and manganese-doped ZnO NPs. The MV dye (molecular formula: $C_{24}H_{28}N_3Cl$, molecular weight: 407.99 g/mol) has an absorbance of $\lambda_{max} = 590$ nm (Figure 1). The MV was used as a model due to its frequent presence in industrial wastes and its health effects [2]. The photocatalytic experiments were carried out in a 500 mL capacity beaker reactor and the mixture of 1 g/L of ZnO, Ag-doped ZnO, and Mn-doped ZnO with 4.5×10^{-4} M MV dye were stirred in the dark for 30 min to allow adsorption/desorption equilibrium before irradiating [16]. The irradiation was then conducted

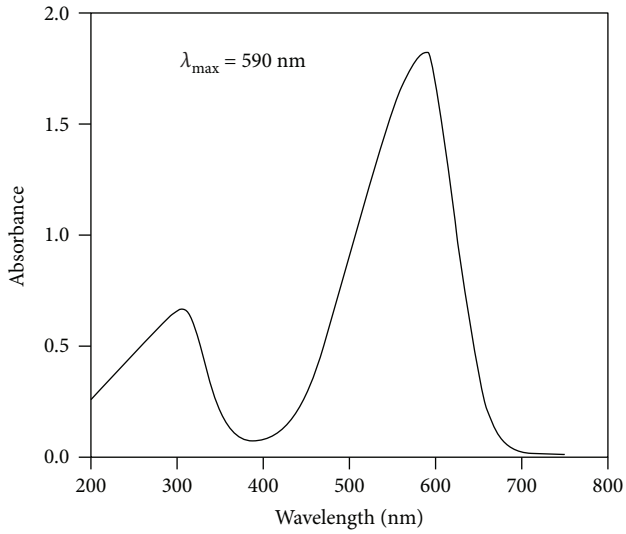

FIGURE 1: The absorbance spectrum of methyl violet.

using sunlight specifically on sunny days in between 10 AM and 2 PM, when the solar intensity fluctuations were minimal [17].

The progress of the photocatalytic decolorization of methyl violet was monitored by withdrawing 10 mL of the sample at 20 min intervals. The suspension was centrifuged at 3000 rpm for 5–7 min and filtered using 0.45 mm Whatman paper to remove the catalyst particles before measuring absorbance. The experiment was repeated with other concentrations and pH levels of the dye solution. The concentration of MV was determined by measuring the absorption intensity at the maximum absorbance wavelength (as measured using a UV-vis spectrophotometer), and percentage of decolorization was calculated from the following equation:

$$\%\text{decolorization} = A_0 - \frac{A_t}{A_0} \times 100, \quad (1)$$

where A_0 is absorbance of dye at initial stage and A_t is absorbance of dye at time "t".

3. Results and Discussion

3.1. XRD Analysis. The X-ray diffraction patterns of ZnO, Mn-doped ZnO, and Ag-doped ZnO are shown in Figure 2. As shown in Figures 2(b) and 2(c), the diffraction patterns of Mn-doped ZnO and Ag-doped ZnO NPs are almost similar to the undoped ZnO NPs except for minor differences probably caused by the presence of tiny impurities of the Ag-doped and Mn-doped ZnO NPs as reported in the JCPDS file number 36-1451. For the Ag-doped ZnO, the existence of silver changed the relative intensity of the diffraction peaks at about 31.80° (100), 34.47° (002), 36.29° (101), 47.58° (102), 56.62° (200), 62.90° (112), 66.40° (103), 67.98° (110), 69.11° (201), and 76.99° (202) as displayed in Figure 2(b). The XRD of Ag-doped ZnO does not show peaks of metallic Ag at 38.21° (111), 44.41° (200), and so on (JCPDS03-092). This may be because of the low dosage of

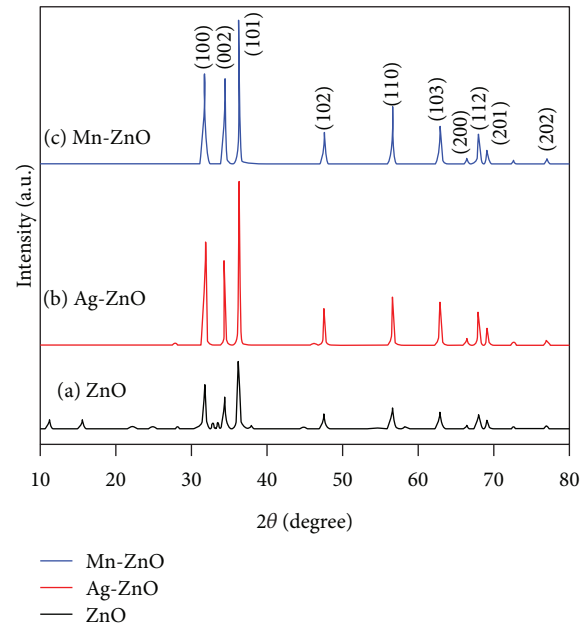

FIGURE 2: The XRD patterns of (a) ZnO, (b) Ag-doped ZnO, and (c) Mn-doped ZnO NPs at 600°C.

silver ions. It might also be due to the O vacancies that were produced from the lower charge of the silver ion-doped ZnO NPs compared with that produced from zinc ions and the formation of a deficiency in silver ion-doped ZnO nanoparticles [7].

For the Mn-doped ZnO, the presence of manganese changed the relative intensity of the diffraction peaks at about 31.79° (100), 34.46° (002), 36.28° (101), 47.57° (102), 56.61° (110), 62.89° (103), 66.39° (200), 67.97° (112), 69.10° (201), and 76.97° (202) as displayed in Figure 2(c). Due to the difference in ionic radii between Zn^{2+} (0.72 Å) and Mn^{2+} (0.80 Å) [18], only a small extent of manganese would be incorporated in the ZnO lattice. This could improve the photocatalytic activity of ZnO, which was verified by the photocatalytic experiments using the MV model dye.

The sharp, definite line broadening of the diffraction peaks positioned at 2θ indicated that the samples are highly crystalline and the synthesized materials are in the nanometer range as it has been reported by others [18]. The crystalline domain size of the synthesized samples of ZnO, Ag-doped ZnO, and Mn-doped ZnO have been obtained from the half width of the full maximum (HWFM) of the most intense peaks of the respective crystals using the Scherrer equation [19].

$$\frac{D = K\lambda}{\beta \cos\theta}, \quad (2)$$

where the constant K is the shape factor = 0.94, λ is the wavelength of X-rays (1.5406 for Cu-Kα), θ is Bragg's angle, and β is the full width at half maximum.

The crystalline domain size of ZnO, Mn-doped ZnO, and Ag-doped ZnO were found to be 31.78 nm, 49.88 nm, and 41.3 nm, respectively. The crystalline domain sizes of Ag-

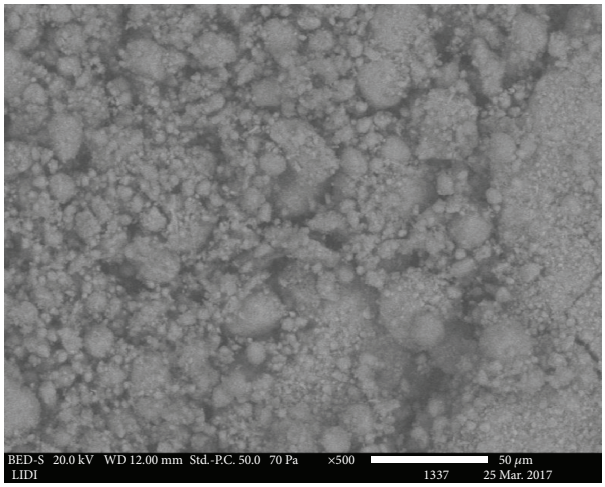

(a)

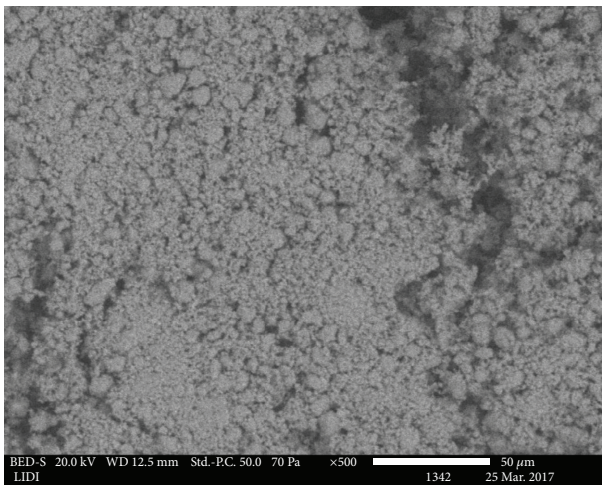

(b)

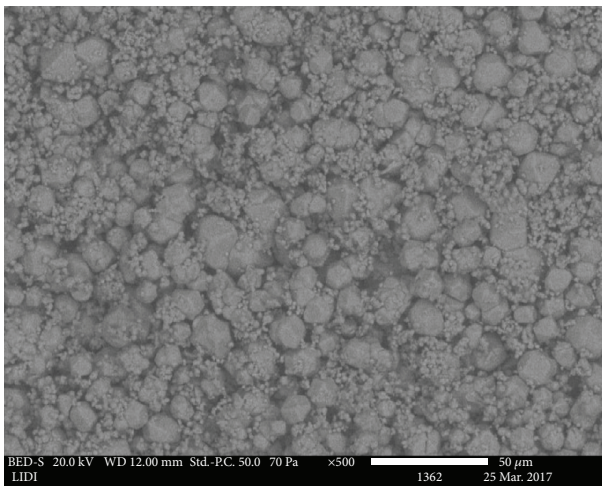

(c)

Figure 3: The SEM micrographs of (a) ZnO, (b) Ag-doped ZnO, and (c) Mn-doped ZnO NPs at 600°C.

doped ZnO and Mn-doped ZnO are larger than ZnO, and this might be due to the anchoring of very small amounts of Ag and Mn at the surface of ZnO, or due to the segregation

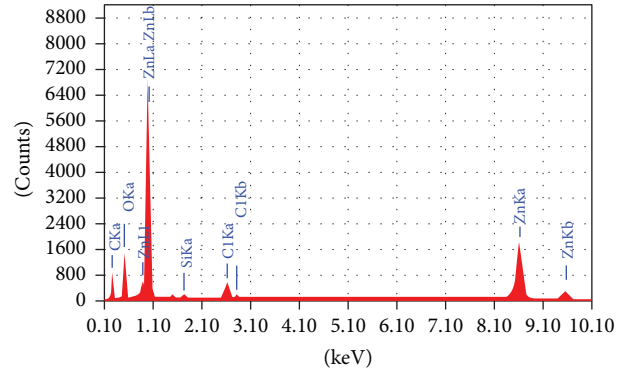

(a)

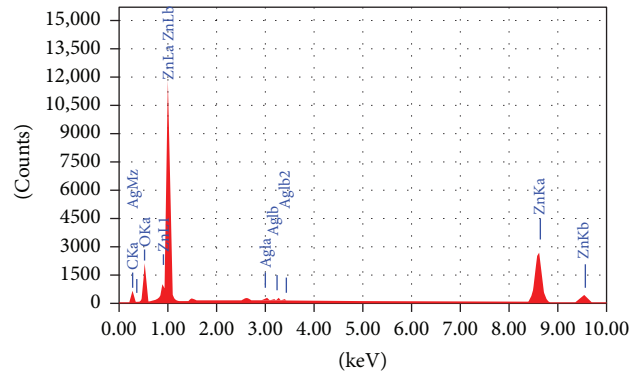

(b)

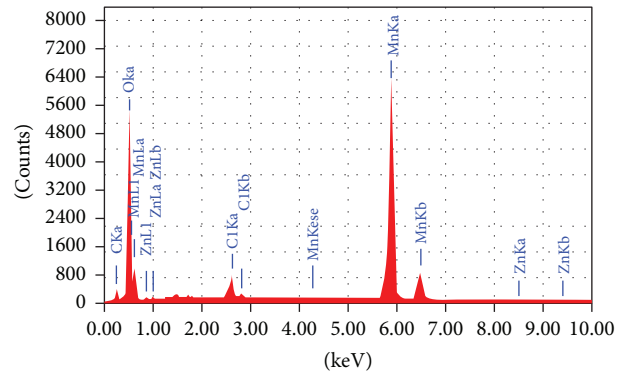

(c)

Figure 4: EDX spectrum of (a) ZnO, (b) Ag-doped ZnO, and (c) Mn-doped ZnO.

of Ag and Mn ions in the boundaries of ZnO [20, 21], or due to the lesser solubility of Mn/Ag in ZnO as reported in [19].

3.2. SEM Analysis. The morphologies of ZnO, Ag-doped ZnO, and Mn-doped ZnO NPs calcined at 600°C are shown in Figure 3. From SEM micrographs, it is evident that the morphology of ZnO changes after doping with Mn and Ag. The SEM micrographs of Mn-doped ZnO and Ag-doped ZnO illustrate that the morphology is relatively ordered and show that the agglomerations of particles are much less in this method of preparation (Figures 3(b) and 3(c)) than in ZnO NPs. Mn and Ag might have disturbed the growth process resulting in the formation of uniformly distributed

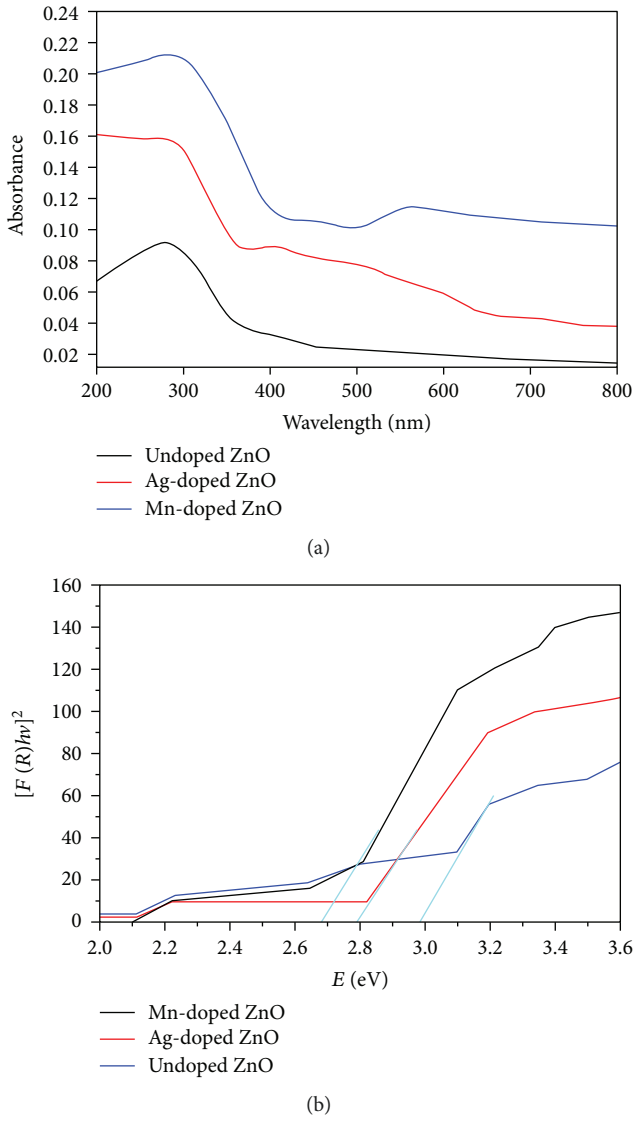

Figure 5: (a) UV-visible absorption spectra and (b) Kubelka-Munk function versus energy plots of ZnO, Ag-doped ZnO, and Mn-doped ZnO NPs at 600°C.

nanosized particles, giving a smooth surface morphology as reported in other studies [18].

Figures 4(a)–4(c) shows the EDX spectrum of ZnO, Ag-doped ZnO, and Mn-doped ZnO NPs. EDX analysis confirmed the presence of manganese and silver in ZnO crystal and some chlorine impurities.

3.3. Optical Analysis. Figure 5(a) shows the UV-visible absorption spectra for ZnO, Mn-doped ZnO, and Ag-doped ZnO NPs. The as-synthesized nanoparticles have a strong absorption maximum below 400 nm. The band gap energy of the nanoparticles is measured by the extrapolation of the linear portion of the graph between the modified Kubelka-Munk function $[F(R)h\nu]^2$ versus photon energy ($h\nu$) [15] as presented in Figure 5(b). The band gap energy of ZnO (2.98 eV) is decreased for Ag-doped ZnO (2.80 eV) and Mn-doped ZnO (2.64 eV). This clearly shows that the improvement of the visible-light absorption is attributed to the presence of metallic Ag and Mn elements that contributes to the narrowing of the band gap of ZnO extending its absorption edge to the visible region to harvesting more photons in the sunlight.

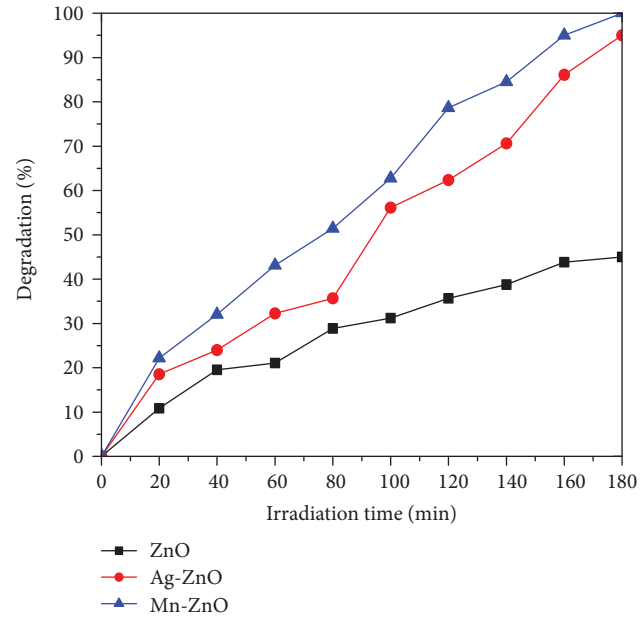

Figure 6: Photocatalytic decolorization of MV using ZnO, Ag-doped ZnO, and Mn-doped ZnO NPs under solar light.

3.4. Photocatalytic Activities of ZnO, Ag-Doped ZnO, and Mn-Doped ZnO NPs. The decolorization percentage of the MV dye (4.5×10^{-4} M) after sunlight irradiation (conducted for 3 hours at a pH of 9.0) of its aqueous solution in the presence of the ZnO, Ag-doped ZnO, and Mn-doped ZnO photocatalysts (1 g/L each) was found to be 45%, 95%, and 100%, respectively (Figure 6). The photocatalytic activity of the ZnO nanoparticles increases by Ag and Mn doping. This might be due to an increase in surface area and oxygen defects [22]. The reaction between conduction band electrons and oxygen in the solution could generate the reactive oxygen species which are responsible for the decolorization [23].

The proposed mechanism of the synergetic effect of Ag-doped ZnO and Mn-doped ZnO NPs on the photocatalytic decolorization of MV has been shown in Figure 7. The valence band electrons in these NPs under sunlight with the photons of energy greater than or equal to ZnO band gap electrons can be excited to the conduction band producing an equal number of holes in the valence band, simultaneously. Because the conduction band energy level of ZnO NPs is higher than that of the intraband state of Ag-doped ZnO and Mn-doped ZnO NPs, electrons can flow from ZnO to Ag^+/Mn^{2+} NPs [24]. So, oxygen vacancy defects and Ag/Mn on the surface of ZnO NPs trap electrons and prevent the recombination of e-h^+ pairs [24]. Also, sunlight

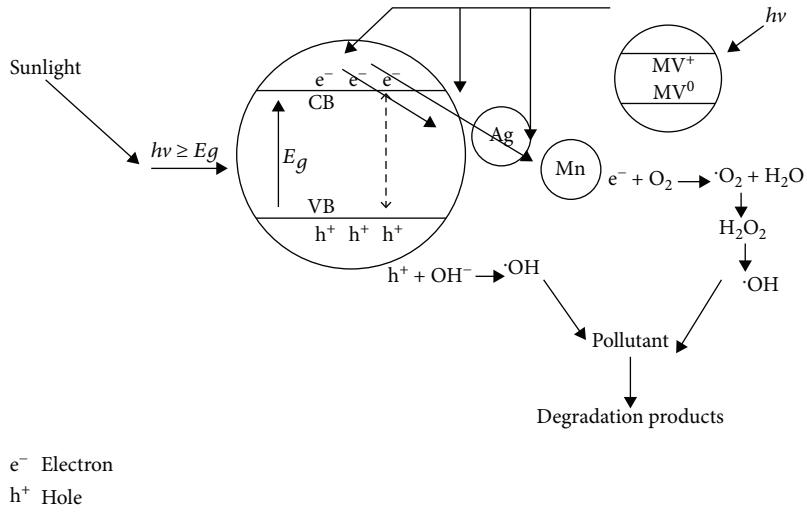

Figure 7: Proposed mechanism for Ag-doped ZnO and Mn-doped ZnO NPs on the photocatalytic decolorization of MV under sunlight.

excites the methyl violet dye molecules (MV^0 to MV^+). The MV molecules transfer electrons to the conduction band (CB) of ZnO (MV^+ to CB of ZnO) and the intraband state of Ag/Mn (MV^+ to Ag/Mn). Here, the intraband state of Mn is lower than Ag; this is why Mn-doped ZnO has a higher photocatalytic efficiency than Ag-doped ZnO.

3.5. Influence of Parameters on the Photocatalytic Decolorization of Methyl Violet

3.5.1. Effect of pH. The role of pH value on the percentage of the photocatalytic decolorization was studied in the pH range of 3–11 at a constant dye concentration of 4.5×10^{-4} M and catalyst amount of 1.0 g/L with the irradiation time of 3 h plotted in Figures 8(a)–8(c). The influence of pH value on the photocatalytic process is the result of a surface charge of ZnO, Ag-doped ZnO, and Mn-doped ZnO and related with the cationic MV dye. The low initial reaction rates at the acidic pH values are due to the photodissolution of the photocatalysts [25]. Since MV is a type of cationic compound, the observed increase of the decolorization percentage at low alkali pH (7 to 9) can be attributed to the high hydroxylation of the catalyst surface. The concentrations of hydroxyl ions in the catalyst surface increased, and the photocatalytic decolorization percentage is improved. However, with a further increase of pH to a value of 11, the photocatalytic decolorization percentage of the MV dye becomes lower. Thus, at a high pH range, electrostatic attraction between the catalyst surface and the MV dye cations leads to a strong adsorption of the dye cations on the ZnO, Ag-doped ZnO, and Mn-doped ZnO NPs in good agreement with other studies [26]. At the high alkali level of pH 11, even though the electrostatic attraction is enhanced, the hydroxyl groups diminish simultaneously. The adsorption of H_2O molecules at the surface of the NPs is followed by the dissociation of OH^- groups, leading to coverage with chemically equivalent metal hydroxyl groups (M-OH) which in turn leads to the decline of photocatalytic decolorization [27]. The maximum photocatalytic decolorization percentage exhibited was at pH 9.0 (Figure 8). pH 9 was used for the next experiments because concentrations of hydroxyl ions in the catalyst surface were increased and decolorization enhanced.

3.5.2. Effect of Catalyst Loading. The photocatalytic decolorization of MV with ZnO, Ag-doped ZnO, and Mn-doped ZnO under sunlight as shown in Figure 9 revealed that, initially, as catalyst loading increased from 0.5 g/L to 1.0 g/L, the photocatalytic decolorization percentage increases. The decolorization percentage exhibited a maximum at 1.0 g/L catalyst dosage because as catalyst loading increases, total active surface area increases; thus, more active sites on the catalyst surface are available and decolorization percentage is increased [28]. Thereafter, as the catalyst loading further increases (from 1 g/L to 2 g/L), the photocatalytic decolorization percentage starts to decrease. This is because of light scattering and screening effects [29]. The tendency of particle-particle interaction increases at a high concentration of catalysts, resulting in a decreasing surface area which is available for sunlight absorption. Finally, the photocatalytic decolorization percentage drops. Even though the number of active sites in solution increases with catalyst loading, a point emerged to be attained where light penetration is compromised due to excessive particle concentration [30]. The tradeoff between these two opposing phenomena results in an optimum catalyst loading for the photocatalytic reaction [31].

3.5.3. Effect of Dye Concentration. The photocatalytic decolorization of the MV was carried out by varying the initial dye concentrations from 4×10^{-4} M to 6×10^{-4} M in order to evaluate the proper amount of initial dye concentration. The results (Figures 10(a)–10(c)) revealed that the initial dye concentration influences the decolorization efficiency rigorously. Initially, as the concentration of the dye increased from 4×10^{-4} M to 4.5×10^{-4} M, the percentage of photocatalytic decolorization by the NPs also increased. However as the initial dye concentration exceeds 4.5×10^{-4} M, the decolorization percentage of the dye decreased sharply. This is due to the fact that a higher initial dye concentration prevents the solar radiation from reaching the catalyst surface (due to the

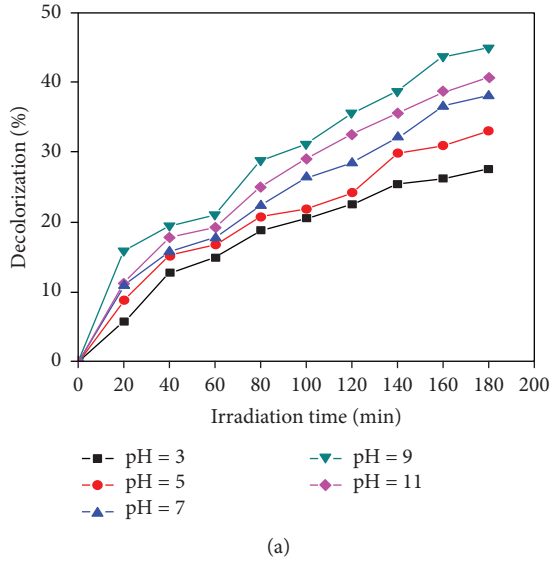

(a)

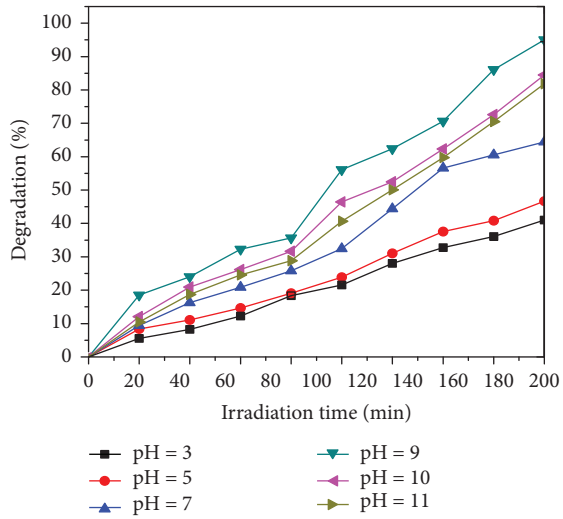

(b)

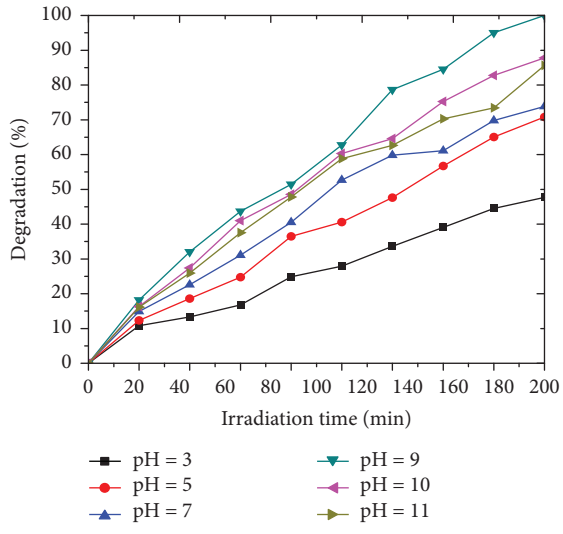

(c)

Figure 8: Effect of pH on decolorization of MV with (a) ZnO, (b) Ag-doped ZnO, and (c) Mn-doped ZnO NPs under sunlight.

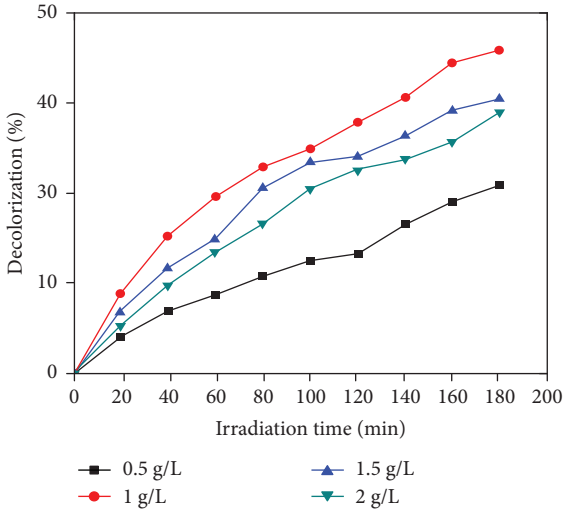

(a)

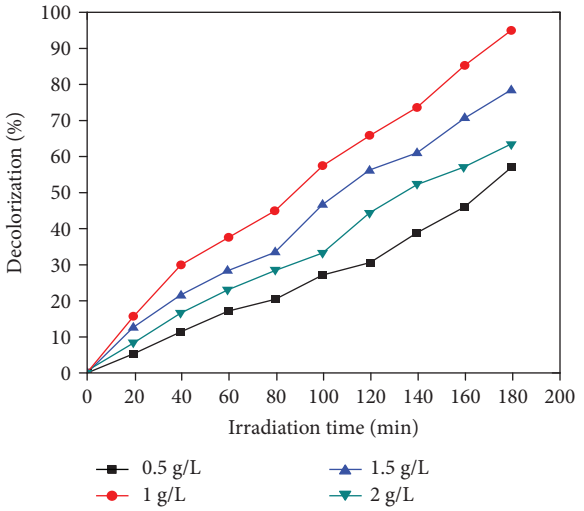

(b)

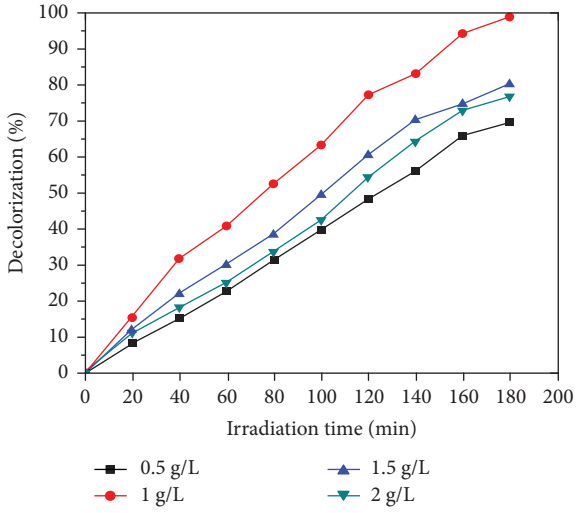

(c)

Figure 9: Effect of catalyst loading on the decolorization of MV with (a) ZnO, (b) Ag-doped ZnO, and (c) Mn-doped ZnO NPs under sunlight.

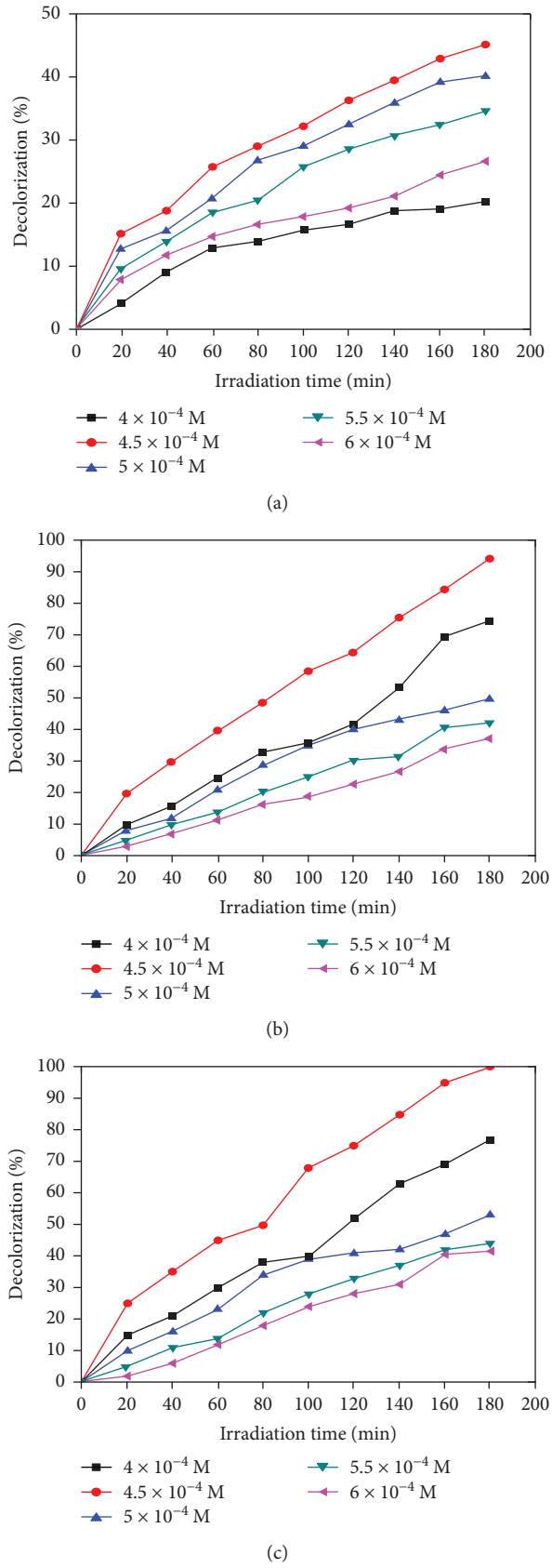

Figure 10: Effect of initial dye concentration on the photocatalytic decolorization of MV under solar light using (a) ZnO, (b) Ag-doped ZnO, and Mn-doped ZnO NPs.

increased path length) and thereby fewer photons reached the catalyst surface. This in turn reduces the production of hydroxyl radicals on the catalyst surface which again implies a reduced attack on the MV dye leading to lower decolorization efficiency [32].

4. Conclusion

In this study, ZnO NPs were synthesized using the precipitation method, and Ag-doped ZnO and Mn-doped ZnO NPs were synthesized using the coprecipitation method. XRD analysis showed that doping of Ag and Mn does not affect the crystal structure of ZnO. UV-vis spectroscopy study reveals that the incorporation of Ag and Mn does not increase the band gap of ZnO but rather decreases it. The EDX spectrum confirmed the presence of manganese and silver in ZnO crystal. Photocatalytic activities of Ag-doped ZnO and Mn-doped ZnO have a higher photocatalytic decolorization efficiency than ZnO. Doped ZnO NPs are promising photocatalysts for water and environmental detoxification.

Data Availability

The XRD, SEM/EDX, Uv-vis, and photocatalytic degradation data used to support the findings of this study are available from the corresponding author upon request.

Conflicts of Interest

The authors declare that they have no conflicts of interest.

Acknowledgments

The authors are especially grateful for the support from the NORAD project (CRPO/CNCS/MU-HU-NMBU/MSc/002/09) and grants from the Mekelle University.

References

[1] Y. Hu and H. Cheng, "Application of stochastic models in identification and apportionment of heavy metal pollution sources in the surface soils of a large-scale region," *Environmental Science & Technology*, vol. 47, no. 8, pp. 3752–3760, 2013.

[2] R. W. Sabnis, Ed., *Handbook of Biological Dyes and Stains: Synthesis and Industrial Applications*, John Wiley & Sons, Hoboken, NJ, USA, 2010.

[3] B. S. Padhi, "Pollution due to synthetic dyes toxicity & carcinogenicity studies and remediation," *International Journal of Environmental Sciences*, vol. 3, no. 3, p. 940, 2012.

[4] E. Forgacs, T. Cserhati, and G. Oros, "Removal of synthetic dyes from wastewaters: a review," *Environment International*, vol. 30, no. 7, pp. 953–971, 2004.

[5] Q. Wan, T. H. Wang, and J. C. Zhao, "Enhanced photocatalytic activity of ZnO nanotetrapods," *Applied Physics Letters*, vol. 87, no. 8, article 083105, 2005.

[6] S. Bhattacharya, I. Saha, A. Mukhopadhyay, D. Chattopadhyay, U. C. Ghosh, and D. Chatterjee, "The role of nanotechnology in water treatment and purification: potential applications and implications," *International Journal of Chemical Science and Technology*, vol. 3, no. 3, pp. 59–64, 2013.

[7] R. Wang, J. H. Xin, Y. Yang, H. Liu, L. Xu, and J. Hu, "The characteristics and photocatalytic activities of silver-doped ZnO nanocrystallites," *Applied Surface Science*, vol. 227, no. 1–4, pp. 312–317, 2004.

[8] C. Xu, L. Cao, G. Su et al., "Preparation of ZnO/Cu_2O compound photocatalyst and application in treating organic dyes," *Journal of Hazardous Materials*, vol. 176, no. 1–3, pp. 807–813, 2010.

[9] M. M. Rashad, A. A. Ismail, I. Osama, I. A. Ibrahim, and A. H. T. Kandil, "Photocatalytic decomposition of dyes using ZnO doped SnO_2 nanoparticles prepared by solvothermal method," *Arabian Journal of Chemistry*, vol. 7, no. 1, pp. 71–77, 2014.

[10] N. Elamin and A. Elsanousi, "Synthesis of ZnO nanostructures and their photocatalytic activity," *Journal of Applied and Industrial Sciences*, vol. 1, no. 1, pp. 32–35, 2013.

[11] R. Ullah and J. Dutta, "Photocatalytic degradation of organic dyes with manganese-doped ZnO nanoparticles," *Journal of Hazardous Materials*, vol. 156, no. 1–3, pp. 194–200, 2008.

[12] M. Joshi, R. Bansal, and R. Purwar, *Color Removal from Textile Effluents*, 2004.

[13] D. Jung, "Syntheses and characterizations of transition metal-doped ZnO," *Solid State Sciences*, vol. 12, no. 4, pp. 466–470, 2010.

[14] C. Karunakaran, V. Rajeswari, and P. Gomathisankar, "Enhanced photocatalytic and antibacterial activities of sol-gel synthesized ZnO and Ag-ZnO," *Materials Science in Semiconductor Processing*, vol. 14, no. 2, pp. 133–138, 2011.

[15] S. Cimitan, S. Albonetti, L. Forni, F. Peri, and D. Lazzari, "Solvothermal synthesis and properties control of doped ZnO nanoparticles," *Journal of Colloid and Interface Science*, vol. 329, no. 1, pp. 73–80, 2009.

[16] S. Yang, Y. Xu, Y. Huang et al., "Photocatalytic degradation of methyl violet with $TiSiW_{12}O_{40}/TiO_2$," *International Journal of Photoenergy*, vol. 2013, Article ID 191340, 5 pages, 2013.

[17] Y. Jiang, Y. Sun, H. Liu, F. Zhu, and H. Yin, "Solar photocatalytic decolorization of C.I. Basic Blue 41 in an aqueous suspension of TiO_2-ZnO," *Dyes and Pigments*, vol. 78, no. 1, pp. 77–83, 2008.

[18] R. Chauhan, A. Kumar, and R. P. Chaudhary, "Photocatalytic studies of silver doped ZnO nanoparticles synthesized by chemical precipitation method," *Journal of Sol-Gel Science and Technology*, vol. 63, no. 3, pp. 546–553, 2012.

[19] K. Rekha, M. Nirmala, M. G. Nair, and A. Anukaliani, "Structural, optical, photocatalytic and antibacterial activity of zinc oxide and manganese doped zinc oxide nanoparticles," *Physica B: Condensed Matter*, vol. 405, no. 15, pp. 3180–3185, 2010.

[20] K. Dhanshree and T. Elangovan, "Synthesis and characterization of ZnO and Mn-doped ZnO nanoparticles," *International Journal of Science and Research*, vol. 4, no. 11, pp. 1816–1820, 2015.

[21] X. Zhou, S. Ge, D. Yao, Zuo, and Y. Xiao, "Preparation, magnetic and optical properties of ZnO and ZnO: Co rods prepared by wet chemical method," *Journal of Alloys and Compounds*, vol. 463, no. 1-2, pp. L9–L11, 2008.

[22] S. M. Hosseini, I. A. Sarsari, P. Kameli, and H. Salamati, "Effect of Ag doping on structural, optical, and photocatalytic properties of ZnO nanoparticles," *Journal of Alloys and Compounds*, vol. 640, pp. 408–415, 2015.

[23] P. Amornpitoksuk, S. Suwanboon, S. Sangkanu, A. Sukhoom, N. Muensit, and J. Baltrusaitis, "Synthesis, characterization, photocatalytic and antibacterial activities of Ag-doped ZnO powders modified with a diblock copolymer," *Powder Technology*, vol. 219, pp. 158–164, 2012.

[24] T. Chen, Y. Zheng, J. Lin, and G. Chen, "Study on the photocatalytic degradation of methyl orange in water using Ag/ZnO as catalyst by liquid chromatography electrospray ionization ion-trap mass spectrometry," *Journal of the American Society for Mass Spectrometry*, vol. 19, no. 7, pp. 997–1003, 2008.

[25] K. Vignesh, A. Suganthi, M. Rajarajan, and S. A. Sara, "Photocatalytic activity of AgI sensitized ZnO nanoparticles under visible light irradiation," *Powder Technology*, vol. 224, pp. 331–337, 2012.

[26] J. Z. Kong, A. D. Li, X. Y. Li et al., "Photo-degradation of methylene blue using Ta-doped ZnO nanoparticle," *Journal of Solid State Chemistry*, vol. 183, no. 6, pp. 1359–1364, 2010.

[27] M. M. Uddin, M. A. Hasnat, A. J. F. Samed, and R. K. Majumdar, "Influence of TiO_2 and ZnO photocatalysts on adsorption and degradation behaviour of erythrosine," *Dyes and Pigments*, vol. 75, no. 1, pp. 207–212, 2007.

[28] M. S. T. Gonçalves, A. M. F. Oliveira-Campos, E. M. M. S. Pinto, P. M. S. Plasência, and M. J. R. P. Queiroz, "Photochemical treatment of solutions of azo dyes containing TiO_2," *Chemosphere*, vol. 39, no. 5, pp. 781–786, 1999.

[29] N. Daneshvar, D. Salari, and A. R. Khataee, "Photocatalytic degradation of azo dye acid red 14 in water on ZnO as an alternative catalyst to TiO_2," *Journal of Photochemistry and Photobiology A: Chemistry*, vol. 162, no. 2-3, pp. 317–322, 2004.

[30] N. Vela, G. Pérez-Lucas, J. Fenoll, and S. Navarro, "Recent overview on the abatement of pesticide residues in water by photocatalytic treatment using TiO_2," in *Application of Titanium Dioxide*, InTech, 2017.

[31] A. Akyol, H. C. Yatmaz, and M. Bayramoglu, "Photocatalytic decolorization of Remazol Red RR in aqueous ZnO suspensions," *Applied Catalysis B: Environmental*, vol. 54, no. 1, pp. 19–24, 2004.

[32] G. Thennarasu and A. Sivasamy, "Enhanced visible photocatalytic activity of cotton ball like nano structured Cu doped ZnO for the degradation of organic pollutant," *Ecotoxicology and Environmental Safety*, vol. 134, Part 2, pp. 412–420, 2016.